Sixth International Symposium on Turbulence and Shear Flow Phenomena
Seoul, Korea, 22-24 June 2009

PDF MODELING STRATEGIES FOR LES OF A BLUFF-BODY STABILIZED SWIRL COMBUSTOR USING PREMIXED GENERATED MANIFOLDS

Clemens Olbricht
Frederik Hahn
Anja Ketelheun
Johannes Janicka
Institute for Energy and Power Plant Technology,
Darmstadt University of Technology
Petersenstr. 30, D-64287 Darmstadt, Germany
ketelheun@ekt.tu-darmstadt.de

ABSTRACT

In this publication a bluff-body stabilized swirled non-premixed methane-air flame of the Sydney flame series is investigated. Large Eddy Simulation (LES) combined with a progress variable approach based on steady laminar premixed flamelets is applied to this configuration. To account for sub grid scale interactions of turbulence and chemistry probability density function (PDF) modeling using presumed β-PDF for the mixture fraction was used. Two different PDF approaches were applied to Premixed Generated Manifolds (PGM). No large differences were observed when using a sufficiently fine numerical grid. Therefore, only one PGM method was studied in more detail with a finer resolution. The comparison with radial velocity and scalar distributions from the experiments shows a good overall agreement.

INTRODUCTION

Large eddy simulation has proven to be a powerful tool for the accurate prediction of transient flow phenomena in technical applications. The main advantage of LES is the resolution of large flow structures containing most of the turbulent kinetic energy. Thus, only the influence of the remaining small scales has to be modeled using sub grid scale (SGS) models. Additional information on the mixture in the subgrid is needed to compute turbulent non-premixed combustion processes. This can be achieved by modeling probability density functions (PDF) for the mixing variables. A variety of different strategies for treating the combustion chemistry and the PDF has been investigated during the last decade. The combination of tabulated chemistry by using steady flamelets with presumed shape β-PDF appears to be very promising as it allows to separate hydrodynamic calculations from the solution of stiff chemical systems. The chemistry computation considering detailed mechanisms in the pre-processing lead to a reasonably low computational cost.

As an extension to the commonly used steady flamelet model to describe the deviations from equilibrium a reaction progress variable has been introduced, for instance by Pierce and Moin (2004). Nevertheless, this model shows a discrepancy by defining a reaction progress for a diffusion flamelet where "mixed is burnt". Vreman et al. (2008) used premixed flamelets in order to create a manifold spanned by the mixture fraction and the progress variable and applied it to non-premixed jet flames. The main advantage of the latter approach consists in the physical description of the chemical sources within the flammable range. In the present work this approach, in the following denoted as *Premixed Generated Manifolds* or briefly PGM, is used in combination with presumed β-PDF modeling.

A study of the swirled CH_4 bluff-body flame SM1 of the Sydney flame series is presented in this publication (Kalt et al., 2002; Al-Abdeli and Masri, 2003). First LES results of flames from this series including SM1 were published by El Asrag and Menon (2007), Stein and Kempf (2007) and, more recently, by Kempf et al. (2008). El Asrag and Menon used a linear eddy mixing model (LEM) combined with a global one-step finite-rate chemistry mechanism, whereas Stein and Kempf and Kempf et al. employed a flamelet tabulation with presumed PDF modeling. These studies revealed problems in accurately predicting the distribution of scalar quantities such as the temperature and chemical species. Shortcomings were attributed to a high sensitivity of the mixture fraction prediction in areas of near-stoichiometric mixtures or the utilization of a simple one-step chemistry.

The next section illustrates the configuration and describes the behavior of the flow. Afterwards the governing equations, the combustion and PDF models and the numerical setup are given. The subsequent section covers the interpretation computational results and a discussion on the performance of the chosen PGM modeling strategies. The last section is devoted to conclusions.

CONFIGURATION

The Sydney bluff-body configuration as investigated in this work consists of a rotationally symmetric bluff body with a diameter of $D_{bb} = 50\,mm$. Fuel, in this case methane at ambient conditions, is fed through a central pipe with $D_j = 3.6\,mm$ with an velocity of $u_j = 32.7\,ms^{-1}$ and a Reynolds number of $Re_j = 7200$. Swirled air (primary air flow) is injected through a $5\,mm$ wide annular gap around the bluff body (axial velocity $u_s = 38.2\,ms^{-1}$, radial velocity $u_s = 19.1\,ms^{-1}$, $Re_s = 75900$). The swirl number S_g

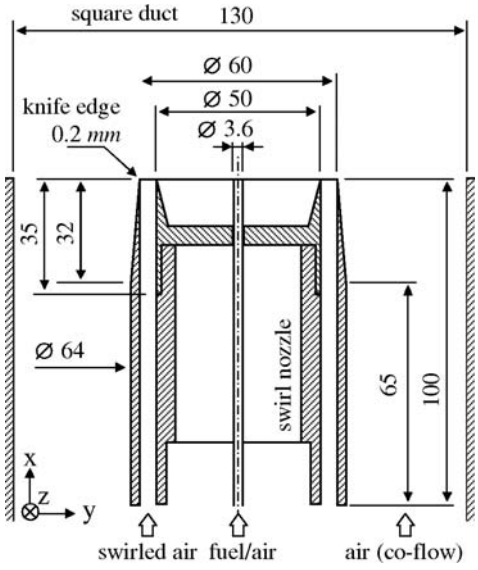

Figure 1: Configuration of the SM burner.

of 0.5 was evaluated with the mean bulk velocities w_s/u_s. The swirl is generated by inclined channels $300\,mm$ upstream of the exit plane. The bluff body is located in a square duct of $130\,mm$ with the secondary air flow at $u_{air} = 20.0\,ms^{-1}$. The configuration with all dimensions and the coordinate system is shown in figure 1. Velocities and velocity fluctuations were measured through laser Doppler velocimetry (LDV), scalar measurements were obtained using Raman/Rayleigh/LIF. The measurements were conducted by Kalt et al. (2002) and Al-Abdeli and Masri (2003).

Computational results of the flame are shown in figure 2 with its instantaneous and mean distributions of the temperature (left figures) and the axial velocity (right figures). The velocity plots show the isoline for $u = 0\,ms^{-1}$. The flame is stabilized by two mechanisms. First, the bluff body acts as geometrical flame holder inducing two counter-rotating vortices forming a recirculation zone in its wake. The lower regions where $u = 0\,ms^{-1}$ close to the bluff body in figure 2 mark these recirculation zones. The inner vortex transports fuel into this zone, while the outer vortex entrains hot gases. Therefore, the fuel is preheated and mixing processes are enhanced. The stoichiometric mixture fraction is very low ($f_{st} = 0.055$), thus the primary reaction zone is situated in the outer shear layer ranging from the outer edge of the bluff body to the region of the strongest lateral contraction. Together with the necking of the flow a region of intense burning establishes close to the stagnation points of the geometrically induced recirculation. Additionally, the outer surface of the bluff body generates vortex shedding influencing the reaction zone and enhancing velocity fluctuations. The second stabilizing mechanism is the swirl induced vortex breakdown bubble (VBB). The VBB establishes a secondary reaction zone further downstream. The downstream isocontour of $u = 0\,ms^{-1}$ shows the position of the VBB. The strong interaction of the fluctuating VBB with the central fuel jet leads to precessing of the jet. The interaction is visualized in the instantaneous velocity distribution in figure 2 where the bounding isolines of zero axial velocity of the vortex breakdown bubble and the recirculation zone interact. In both the instantaneous temperature and velocity field the precessing fuel jet can be observed.

MODELING AND NUMERICS

This section gives an overview of the filtered LES equations, the premixed generated manifolds method and the PDF modeling applied within. At the end, the numerical procedure for solving these equations and the numerical setup of the configuration is described.

LES modeling

In configurations with relatively low flow velocities, the density can be assumed independent of the pressure. It only varies due to changing of the temperature and the scalar composition. The following equations represent the Favre-filtered (density weighted filtering: $\overline{\rho}\widetilde{\phi} = \overline{\rho\phi}$) equations for mass, momentum and a scalar φ:

$$\frac{\partial \overline{\rho}}{\partial t} + \frac{\partial}{\partial x_j}\left(\overline{\rho}\widetilde{u_j}\right) = 0 \tag{1}$$

$$\begin{aligned}\frac{\partial}{\partial t}\left(\overline{\rho}\widetilde{u_i}\right) + \frac{\partial}{\partial x_j}\left(\overline{\rho}\widetilde{u_i}\widetilde{u_j}\right) = \frac{\partial}{\partial x_j}\Bigg(\overline{\rho\nu}\Bigg(\frac{\partial \widetilde{u_i}}{\partial x_j} + \cdots \\ \frac{\partial \widetilde{u_j}}{\partial x_i} - \frac{2}{3}\frac{\partial \widetilde{u_k}}{\partial x_k}\delta_{ij}\Bigg) + \overline{\rho}\tau_{ij}^{sgs}\Bigg) - \frac{\partial \overline{p}}{\partial x_i} + \overline{\rho}g_i\end{aligned} \tag{2}$$

$$\begin{aligned}\frac{\partial}{\partial t}\left(\overline{\rho}\widetilde{\varphi}\right) + \frac{\partial}{\partial x_j}\left(\overline{\rho}\widetilde{u_j}\widetilde{\varphi}\right) = \cdots \\ \frac{\partial}{\partial x_j}\left(\overline{\rho}\left(\widetilde{D_\varphi}\frac{\partial \widetilde{\varphi}}{\partial x_j} + J_{\varphi,j}^{sgs}\right)\right) + \widetilde{S_\varphi}\end{aligned} \tag{3}$$

The subfilter fluxes of momentum and scalars τ_{ij}^{sgs} and $J_{\Phi,j}^{sgs}$, appearing in the equations above due to the filtering operations, have to be modeled. The subgrid scale stress tensor τ_{ij}^{sgs} is closed by the standard Smagorinsky model. The deviatoric part is modeled based on an eddy-viscosity assumption, while the isotropic part is included in the pressure term, resulting in the pressure parameter.

$$\tau_{ij}^{sgs} - \frac{1}{3}\tau_{kk}^{sgs}\delta_{ij} \approx 2\nu_t\widetilde{S_{ij}} \tag{4}$$

$$\text{with} \quad \nu_t = \left(C_S\bar{\Delta}\right)^2\left|\widetilde{S_{ij}}\right| \tag{5}$$

$$\widetilde{S_{ij}} = \frac{1}{2}\left(\frac{\partial \widetilde{u_i}}{\partial x_j} + \frac{\partial \widetilde{u_j}}{\partial x_i}\right) \tag{6}$$

The coefficient C_S in equation (5) is obtained by the dynamic procedure of Germano et al. (1991). $\bar{\Delta}$ denotes the LES filter width.

The scalar fluxes $J_{\varphi,j}^{sgs}$ in equation (3) are modeled consistently with the sub grid stresses with a gradient approach.

$$J_{\varphi,j}^{sgs} \approx \frac{\nu_t}{\sigma_t}\frac{\partial \widetilde{\varphi}}{\partial x_j} \tag{7}$$

The turbulent Schmidt number $\sigma_t = 0.7$ relates the turbulent diffusion coefficient to the turbulent viscosity.

Combustion Modeling

The combustion modeling used in this work is based on a flamelet approach, describing the turbulent three-dimensional flame front by a set of laminar steady one-dimensional flamelets. The progress variable approach used in this work follows the work of van Oijen (2002) and others. It combines flamelets with a reaction progress variable accounting for finite-rate chemistry effects. A set of premixed flamelets for different mixture fractions f was computed using the laminar flame code Chem1D with the GRI 3.0 reaction mechanism. The progress variable $\mathcal{Y}$ must be strictly monotonical along the flamelet. In the context of

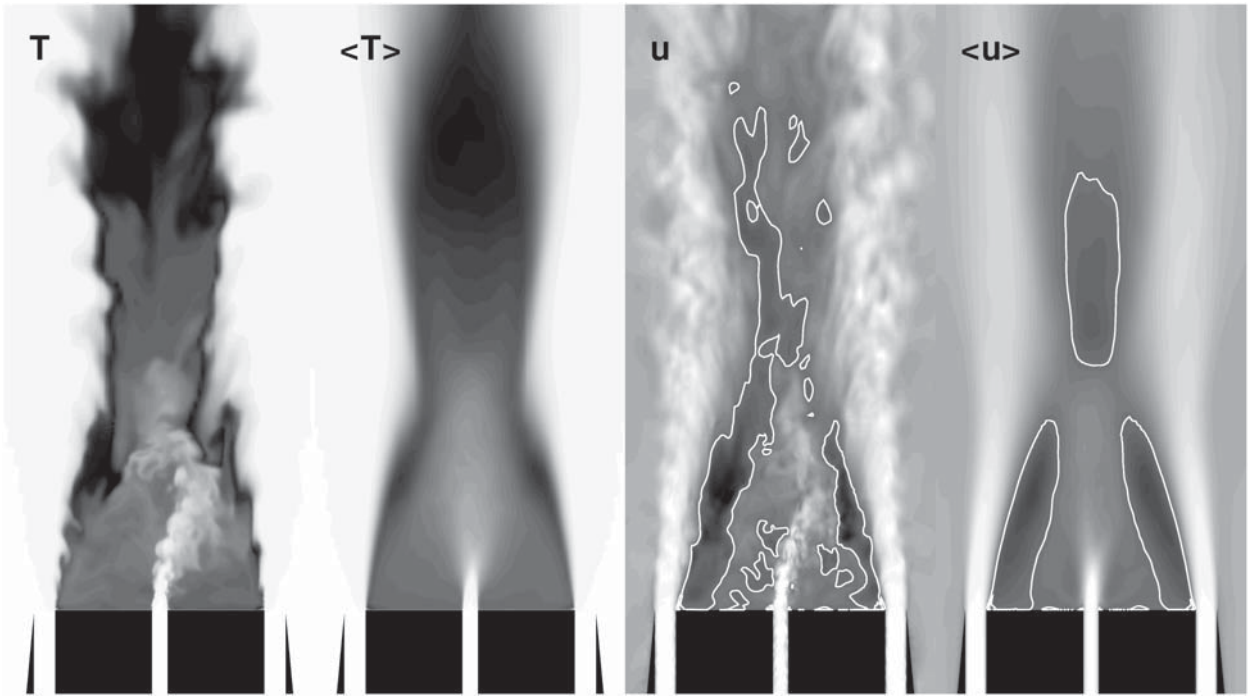

Figure 2: Instantaneous and mean temperature and axial velocity distribution taken from the computation employing 4 million grid points. The coloring ranges from $300\,K$ (white) to $2100\,K$ (black), resp. -20 (black) to $40\,ms^{-1}$ (white).

this work, the species mass fraction of CO_2 has been chosen ($\mathcal{Y} = Y_{CO_2}$). Albeit the simplicity of this choice CO_2 is fairly sensitive in a wide range of the flame.

Since no solutions outside the flammability limits (approx. $f < 0.02$ and $f > 0.1$) can be obtained, an extrapolation was performed to fill the whole range of mixture fractions from 0 to 1. For this publication, a technique considering the thermo-chemical behavior of each variable has been chosen. Species mass fractions Y_i and hence the progress variable are extrapolated linearly. The density ρ and the species' molar masses M_i follow a hyperbolic law for mixing. To fulfil the perfect gas equation, the temperature was calculated accordingly (see Ketelheun et al., 2009).

In this work, the temperature, species mass fractions, as well as the density and the viscosity are tabulated as functions of the mixture fraction and the reaction progress variable which are transported following equation (3). The manifold reads as:

$$\Phi = \Phi\left(f, \mathcal{Y}\right) \tag{8}$$

The filtered variables are obtained by integration over a density weighted sub grid PDF of the controlling variables.

$$\widetilde{\Phi\left(f,\mathcal{Y}\right)} = \iint \Phi\left(f,\mathcal{Y}\right) P\left(f,\mathcal{Y}\right)\, \mathrm{d}f\, \mathrm{d}\mathcal{Y} \tag{9}$$

To model the joint PDF $P\left(f,\mathcal{Y}\right)$ two different assumptions on the statistical independence of mixture fraction and progress variable have been used. The first approach, called PGM1 in the remainder of this work, assumes independence of f and $\mathcal{Y}$.

$$P\left(f,\mathcal{Y}\right) = P\left(f\right) \cdot P\left(\mathcal{Y}\right) \tag{10}$$

The second approach, called PGM2, is based on a method by Landenfeld et al. (2002). They propose a normalization procedure for the progress variable to minimize the statistical dependence of f and $\mathcal{Y}$ in flames burning near equilibrium. Neglecting cross-correlations according to Landenfeld et al. (2002) the normalized progress variable is defined as:

$$C = \frac{\mathcal{Y}}{\mathcal{Y}_{max}} \quad \text{and} \quad \widetilde{C} \approx \widetilde{\mathcal{Y}} \cdot \left(\widetilde{\frac{1}{\mathcal{Y}_{max}}}\right) \tag{11}$$

In both methods PGM1 and PGM2 the PDF of the mixture fraction is modeled as β-function. Conceptually the β-function is unsuitable for premixed flame situations in LES represented by the (scaled) reaction progress variable. Thus, it is modeled using a Dirac δ-function. This approach is appropriate due the approximately piecewise linear relationship of the progress variable and the thermo-chemical state together with high grid resolutions. A possible slight shift in the effective burning velocity is uncritical for the modeling of SM1 since the flame stabilization is based on recirculation of hot gases and not on premixed flame propagation.

The sub grid variance of the mixture fraction is modeled according to:

$$\widetilde{f''^2} = C_2 \bar{\Delta}^2 \frac{\partial \widetilde{f}}{\partial x_j} \frac{\partial \widetilde{f}}{\partial x_j} \quad \text{with} \quad C_2 = 0.15 \tag{12}$$

Numerical Procedure and Setup

All the governing equations were implemented in the three-dimensional CFD code FASTEST-ECL. The code uses geometry-flexible, blockstructured, boundary fitted grids. This enables FASTEST-ECL to represent complex geometries such as the one investigated here. A collocated grid with a cell-centered variable arrangement is used. The flow solver offers fully second order accuracy. Discretization is based on the finite volume method. For spatial discretization specialized central-differencing schemes are used. To assure boundedness of the mixture fraction, the convective term in the scalar transport equation (3) was discretized using non-oscillatory bounded TVD schemes. For the time stepping multiple stage Runge-Kutta schemes (here: three

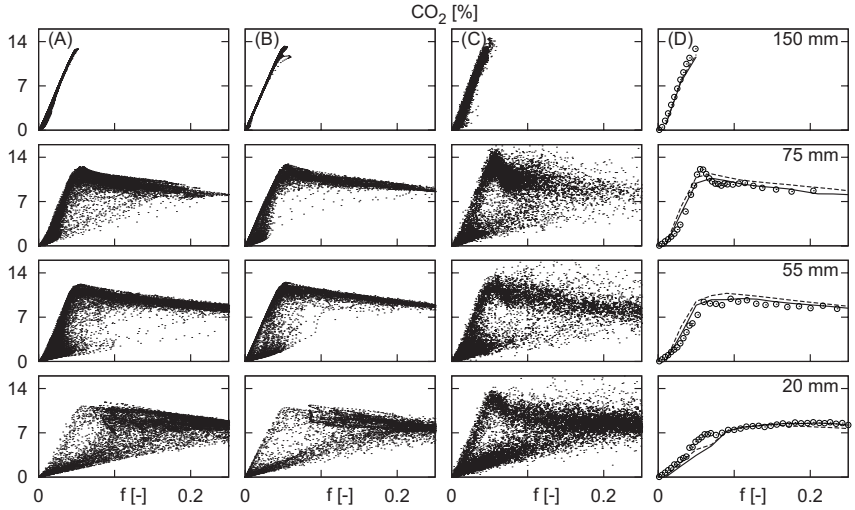

Figure 3: Scatter plot for CO_2 mass fraction. (A) PGM1, (B) PGM2, (C) experimental data, (D) conditional means from scatter plots with ' ⊙ ' experiments by Al-Abdeli and Masri (2003), ' — ' LES/PGM1, ' – – ' LES/PGM2 (both LES with 2.2 million grid points).

stages) with second order accuracy were used. Following a fractional step formulation, in each stage a momentum correction is carried out in order to satisfy the continuity. For further details see Hahn et al. (2008).

The computations were carried out on elliptically smoothed hexahedral grids with $2.2 \cdot 10^6$ and $4 \cdot 10^6$ grid points, respectively. Special three-dimensional O-grid structures were used to obtain very fine resolutions within the fuel jet, around the bluff body and close to the nozzle. The computational domain covers the square duct in the lateral direction and includes the nozzle for one bluff body diameter ($1D_{bb} \approx 13.8D_j$) upstream. Downstream, the domain covers about $10D_{bb}$. The calculations confirm that the flame fits in the computational domain. For the inlet conditions the bulk flows were prescribed for the jet and the primary air flow. For the co-flow artificial turbulence was superimposed using the method of Klein et al. (2003) with a lengthscale of $4 - 8\,mm$. The turbulence intensity was chosen to be 5%.

The chemical database was resolved with $901 \times 101 \times 11$ entries for mixture fraction, reaction progress variable and mixture fraction variance, respectively. The data was equidistantly distributed in order to have a fast and search free table access. The fine resolution is necessary to accurately capture the very small flammable region of the fuel.

RESULTS

As a preliminary study of the methods PGM1 and PGM2 computations on a smaller grid with 2.2 million grid points were carried out and scatter plots of the CO_2 mass fractions were compared with each other and experimental data. In the second part of this section the method PGM2 is investigated more closely and the radial means of velocities and scalars are compared to the experiments. A description of the flame behavior and the effects present in the flame were given in the beginning of this publication, accompanied by figure 2.

Scatter Plots

Figure 3 shows events of the CO_2 mass fraction plotted against the mixture fraction at different axial positions. Due to the incorporation of premixed laminar flames (varying from unburnt to burnt states) into the chemical databases the PGM combustion model includes the non-reacting mixing regime as well as the burnt regime. Since the main portion of scalar transport is resolved the PGM model together with LES is per se appropriate to account for resolved blow-off events. In contrast to that issue, quenching based on sub grid strain is not included in the used methodology.

As it is shown by figure 3 both PDF modeling strategies account for extinction effects. This is demonstrated by very low values of the transported quantity CO_2 within the flammable regions. Both methods represent the experimental distribution with respect to shape and probability reasonably well. The scattered data and the conditional means in column (D) show slightly better results for PGM1. This is caused by the effect of the different PDF modeling strategies on the source term of the progress variable CO_2. The assumption of statistical indepence of the mixture fraction and the physical progress variable seems to be better suited for flame SM1 with strong deviations from chemical equilibrium and massive local extincion. Nevertheless the two methods do not differ much in the prediction quality using a high grid resolution accompanied by narrow PDFs in the region of interest. Therefore, the PGM2 method has been chosen for a more detailed investigation of the flow and scalar field with further increased grid resolution.

Radial Distribution

Figure 4 shows the time averaged results of the LES with four million grid points and the combustion modeling strategy PGM2 at different axial positions for the axial and rotational velocity components as well as their fluctuations compared to experimental data. Overall, a good agreement with the experimental data could be achieved, albeit an incorrect slight shift of the experimental data towards higher radii is evident. This results for instance in a measured angular momentum at the symmetry axis.

The main flow features like the spreading mechanism and the recirculation of highly rotating hot gas towards the burner's base are well captured by the LES. The position of the stagnation point for the bluff body recirculation zone

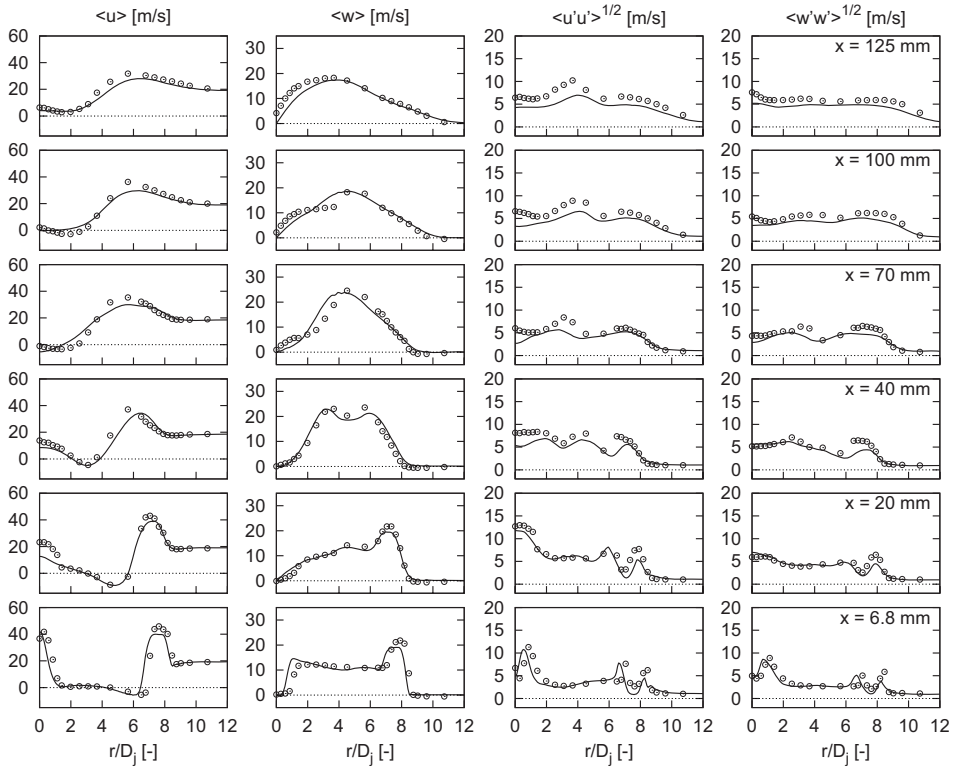

Figure 4: Time averaged results for axial and rotational velocity means and fluctuations. ' ⊙ ' Experiments by Al-Abdeli and Masri (2003), ' — ' LES/PGM2 with four million grid points.

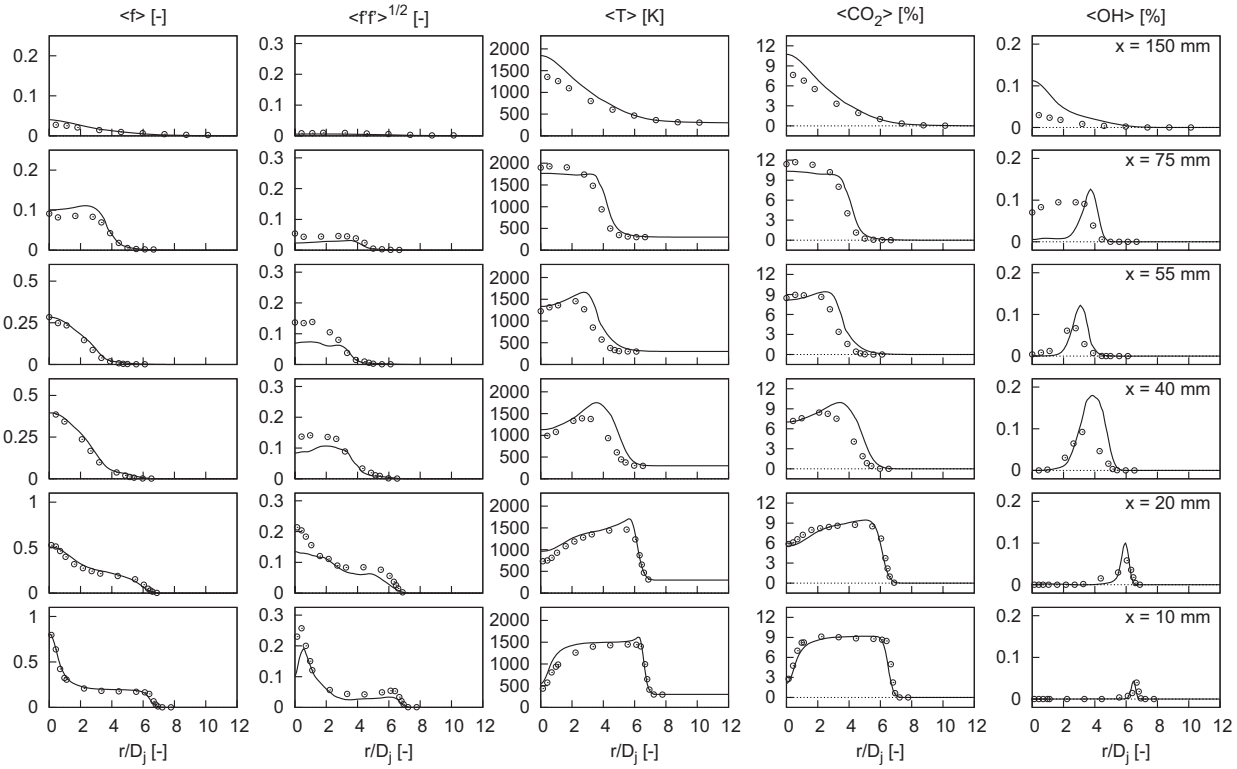

Figure 5: Time averaged results for mixture fraction, mixture fraction fluctuation, temperature and species mass fractions. ' ⊙ ' Experiments by Al-Abdeli and Masri (2003), ' — ' LES/PGM2 with four million grid points.

was given by the experimental results of Kalt et al. (2002) at a position 43 mm downstream of nozzle. The stagnation point in the computation was found at 45 mm. The vortex breakdown bubble was observed in the experiment between $x = 65$ and 100 mm, in the simulation between $x = 58$ and 103 mm.

However, the jet penetration is not perfectly matched, as it is observed at the axial stage at $x = 20\,mm$. At measurement planes further downstream where the vortex breakdown bubble is located slight deviations occur. The fluctuations of both components are well captured in both their shape and position of the peak values. Even though artificial turbulent data were not prescribed at the fuel and the swirled air inlet the vortex shedding mechanisms are well predicted by the LES benefiting from the inclusion of the nozzle in the computational domain and the refinement strategy using three-dimensional O-grids within the nozzle.

In figure 5 the time averaged results for the mixture fraction, its fluctuation, the temperature, CO_2 and OH mass fractions are given. The mean values of the mixture fraction match very well with the experimental results in most parts of the domain. The mixture fraction profile at $x = 75\,mm$ suggests that diffusion effects might be too low due to a too high value of the turbulent Schmidt number. The temperature at $x = 10\,mm$ is somewhat too high, mainly in the rich parts of the flame. This can be explained by effects from the tabulation method. Due to the use of premixed flamelets no diffusion in mixture fraction space is included. Therefore, the peak values of the temperature in the chemistry table are higher than for non-premixed flamelets. The extrapolation routine may cause additional differences. Other authors (cf. Olbricht et al., 2008; Kempf et al., 2008) using standard steady flamelet approaches have shown a peak of the temperature and very high amounts of OH on the outer edge of the bluff body where the flame front is situated. In the present computation the peak is present as well, but it is considerably lower, OH is very well captured. This effect can be explained by a better description of the heat release in the flame.

CONCLUSION

In this publication a swirled methane flame has been investigated by LES with premixed generated manifolds chemistry tabulation. Two different approaches for modeling the mixture fraction PDF were considered. Scatter plots of the CO_2 mass fraction demonstrated that the PGM methodology is well suited to capture extinction events in the absence of modeling sub grid scale quenching. It turned out that assuming statistical independence of the mixture fraction and the physical progress variable within the modeling of the joint PDF results in slightly better results than implying a fixed dependency according to Landenfeld et al. (2002). Nevertheless, only marginal differences between both approaches can be observed as long as the grid resolution is sufficiently fine. One of the approaches has been chosen for further investigations. The radial profiles of the LES results are in very good accordance to the experimental data. The LES/PGM method has been successfully applied to this complex swirl configuration.

ACKNOWLEDGEMENT

The LES computations were performed on the Hessian High Performance Computer (HHLR), which is supported by the High Performance Scientific Computing (HPSC) activity group, a member of the computational engineering center (FZCE) in Darmstadt. The authors gratefully acknowledge the "*German Research Foundation (DFG)*" for financial support through the collaborative research center 568.

REFERENCES

Y. M. Al-Abdeli and A. R. Masri. Stability characteristics and flowfields of turbulent non-premixed swirling flames. *Combust. Theory Modelling*, 7:731–766, 2003.

H. El Asrag and S. Menon. Large eddy simulation of bluff body stabilized swirling non-premixed flames. *Proc. Combust. Inst.*, 31:1747–1754, 2007.

M. Germano, U. Piomelli, P. Moin, and W. H. Cabot. A dynamic subgrid-scale eddy viscosity model. *Phys. Fluids A*, 3(7):1760–1765, 1991.

F. Hahn, C. Olbricht, and J. Janicka. Study of various configurations under variable density mixing conditions aiming on gas turbine combustion using LES. *ASME Turbo Expo: Power for Land, Sea and Air*, 2008. GT2008-50268.

P. A. M. Kalt, Y. M. Al-Abdeli, A. R. Masri, and R. S. Barlow. Swirling turbulent non-premixed flames of methane: flow field and compositional structure. *Proc. Combust. Inst.*, 29:1913–1919, 2002.

A. Kempf, W. Malalasekera, K. K. J. Ranga-Dinesh, and O. Stein. Large eddy simulations of swirling non-premixed flames with flamelet models: A comparison of numerical methods. *Flow, Turb. Combust.*, 81:523–561, 2008.

A. Ketelheun, C. Olbricht, F. Hahn, and J. Janicka. Premixed generated manifolds for the computation of technical combustion systems. *ASME Turbo Expo: Power for Land, Sea and Air*, 2009. GT2009-59940, accepted for publication.

M. Klein, A. Sadiki, and J. Janicka. A digital filter based generation of inflow data for spatially developing direct numerical or large eddy simulation. *J. Comput. Physics*, 186:652–665, 2003.

T. Landenfeld, A. Sadiki, and J. Janicka. A turbulence-chemistry interaction model based on a multivariate presumed beta-pdf method for turbulent flames. *Flow, Turb. Combust.*, 68:111–135, 2002.

C. Olbricht, F. Hahn, and J. Janicka. Detailed numerical investigation of sydney bluff-body flames. *Proc. Eng. Turb. Model. Meas.*, 7:713–718, June 2008.

C. D. Pierce and P. Moin. Progress-variable approach for large-eddy simulation of non-premixed turbulent combustion. *J. Fluid Mech.*, 504:73–97, 2004.

O. Stein and A. Kempf. LES of the sydney swirl flame series: A study of vortex breakdown in isothermal and reacting flows. *Proc. Combust. Inst.*, 31:1755–1763, 2007.

J. A. van Oijen. *Flamelet-Generated Manifolds: Development and Application to Premixed Laminar Flames.* Ph.D. Thesis, TU Eindhoven, 2002.

A. W. Vreman, B. A. Albrecht, J. A. van Oijen, L. P. H. de Goey, and R. J. M. Bastiaans. Premixed and non-premixed generated manifolds in large-eddy simulation of Sandia flame D and F. *Combust. Flame*, 153:394–416, 2008.